sustainability

MDPI

Article

Influence of the Ground Greening Configuration on the Outdoor Thermal Environment in Residential Areas under Different Underground Space Overburden Thicknesses

Xiaochao Su [1,2], Hao Cai [2,*], Zhilong Chen [1,2,*] and Qilin Feng [2]

1 Underground Space Research Center, Army engineering university of PLA, Nanjing 210007, China; suxiaochao025@163.com

2 State Key Laboratory of Explosion & Impact and Disaster Prevention & Mitigation, Army Engineering University of PLA, Nanjing 210007, China; fengqilin891109@gmail.com

* Correspondence: chen-zl@vip.163.com (Z.C.); caihaohvac@gmail.com (H.C.); Tel.: +86-25-80825101 (Z.C.); +86-25-80825385 (H.C.)

Received: 17 August 2017; Accepted: 14 September 2017; Published: 18 September 2017

Abstract: In the underground space development of residential areas, outdoor thermal environments at the pedestrian level greatly depend on the ground greening configuration, which is in turn affected by the overburden thickness of the underground space (OTUS). However, few studies have considered the effects of OTUS on the ground greening configuration and the further effects of the ground greening configuration on the outdoor thermal environment. This study aimed to provide insights into the design of OTUS for improving outdoor thermal environments. Two residential areas with row and enclosed layouts in Nanjing, China, were numerically studied using the computational fluid dynamics (CFD) simulation software ENVI-met. Outdoor thermal environments in the two residential areas, which had the same greening coverage rate, were simulated under different OTUSs and ground green configurations. The results indicate that to create a comfortable outdoor thermal environment, the OTUS should be designed to satisfy the requirement for planting small trees. If this requirement cannot be adequately satisfied, individuals can also set up tree wells or add soil on top of underground structures to plant small trees, and establish an OTUS that can satisfy the requirement of planting large shrubs in other areas.

Keywords: underground space; overburden thickness; residential area; greening configuration; outdoor thermal environment

1. Introduction

In recent years, with the rapid development of urbanization in China, there have been increasing problems related to the urban heat island effect during summer [1,2]. The urban heat island effect can reduce the outdoor thermal comfort of urban residents [3,4], increase the energy consumption from air conditioning in buildings [2,5], and even lead to fatalities [6–9]. Between 1989 and 2000, the peak mortality rate in America during summer was 5.7%, which was partly caused by the heat island effect, exceeding the total number of deaths caused by hurricanes, floods, and tornadoes [6].

Summer heat problems in residential areas have received considerable attention because these areas are the main places where urban residents live and perform outdoor activities [1,10]. Planners and designers have focused on outdoor greening to mitigate the heat island effect [1]. Increasing ground greening coverage can effectively mitigate the heat island effect by providing shade and reducing the surface temperatures of the ground and buildings [2,3,11–13]. In addition, optimizing the greening configurations can also improve the outdoor thermal and wind environments [10,14,15]. Several

studies have revealed that trees are more effective than grasses in improving outdoor pedestrian comfort [16,17]. The air temperature at the pedestrian level can be reduced by approximately 1 °C by having a tree area that accounts for more than 1/3 of the land area [18]. Although the influence of residential greening on outdoor thermal environments has been studied extensively, few studies have qualitatively discussed the influence of underground space development on residential greening and outdoor thermal environments [19–22] and even fewer have discussed this topic quantitatively [23,24].

Currently, the development and utilization of underground space has become ubiquitous in residential areas. By transferring some ground-level building spaces with lower environmental requirements to underground spaces, more ground area can be reserved for greening and waterscapes, which can further improve the outdoor thermal environment. In our previous studies, we quantitatively analyzed the changes in outdoor thermal environments before and after the development of underground space in a residential area in Nanjing, China, using the computational fluid dynamics (CFD) simulation software ENVI-met [23,24]. This study quantified the effects of increasing the ground greening area on outdoor thermal environments by transferring the parking lot to an underground space in the residential area. However, this study did not consider the effects of the overburden thickness of underground space (OTUS) on the ground greening configuration and consequently the effects of the ground greening configuration on the outdoor thermal environment.

In the underground space development areas of a residential area, the OTUS greatly affects the ground greening configurations. The OTUS requirements ascend in the order of grasses, shrubs, and trees. An insufficient OTUS can limit plant growth and further reduce the positive effects of ground greening on improving outdoor thermal environments. Therefore, the OTUS should be considered as an important factor for creating a comfortable outdoor environment.

This study aims to provide insights into the design of OTUS for improving outdoor thermal environments. Two residential areas with determinant and enclosed layouts in Nanjing, China, were taken as the research objects. We quantitatively studied the outdoor thermal environments in the two residential areas with the same greening coverage rate under different OTUS and ground green configurations using the CFD simulation software ENVI-met. Compared to our previous studies [23,24], this study fully considered the effects of OTUS on the ground greening configuration and the further effects of the ground greening configuration on the outdoor thermal environment. In addition, on the basis of the simulation results, this study revealed the influence mechanism of the OTUS on the outdoor thermal environment and provided several suggestions for underground space development in residential areas.

2. Influence Mechanism of the Overburden Thickness of Underground Space on the Ground Greening Configuration and Outdoor Thermal Environment of Residential Areas

2.1. Influence of the Overburden Thickness of Underground Space on the Ground Greening Configuration

The OTUS determines the ground greening configurations in the development area. According to the current specifications and engineering experience, the requirements for different plant growths on the OTUS are listed in Table 1. If the OTUS is not sufficient for growing shrubs or tall trees, the landscape will be monotonous, and the outdoor thermal environment may also be unsatisfactory.

Table 1. Overburden thickness of underground space required for the growth of different plants.

Plant Types		Height (m)	Typical Plants	Overburden Thickness of Underground Space (mm)		
				Reference [25]	Reference [26]	Engineering Experience
Trees	Small Trees	6–10	Osmanthus	—	>900	800–1000
	Large Trees	20–30	Camphor	900–1200	>1500	1200–1500
Shrubs	Small Shrubs	1–1.5	Golden leaf privet	300–400	>450	300–450
	Large Shrubs	1.5–3	Phnom Penh	450–600	>600	450–600
Land Vegetation		0.2–1	Grass	100–200	>300	150–300

2.2. Mechanism of Greening on the Community Thermal Environment

Many studies have shown that greening can effectively improve the outdoor thermal environment [11,18,27–30]. First, tall trees can block solar radiation, which can significantly reduce the surface temperature of buildings and thus reduce the long-wave heat radiation from the buildings to the surrounding environment [11]. Second, through photosynthesis and transpiration, the land vegetation can moderate solar heat gain on the land and can thus reduce the land temperature and long-wave heat radiation from the land to the surrounding environment [30–32]. In addition, a proper greening layout can improve outdoor ventilation and strengthen convective heat transfer [1,15,17]. The possible effects of different types of plants on the outdoor thermal environment in a residential area are discussed in Table 2.

Table 2. Possible effects of different types of plants on the outdoor thermal environment in a residential area.

Plant Type	Thermal Environment Parameters			
	Air Temperature	Wind Environment	Radiation	Relative Humidity
Large Trees	Reduce solar heat gains by shading; absorb the majority of the heat and reduce the air temperature by photosynthesis and transpiration	Reduce the wind speed at high elevations via the plant canopy and introduce airflow from high elevations to the pedestrian height	Shade, absorb and reduce long-wave radiation	Increase the level of humidity via plant transpiration
Small Trees				
Large Shrubs		Affect the wind environment at the pedestrian height	Partially shade, absorb and reduce long-wave radiation	
Small Shrubs	Reduce land heat storage and strengthen the heat emission of soil; reduce the land surface temperature and air temperature	Typically do not affect the wind environment	Reduce the ground absorption of solar radiation and reduce long-wave radiation from ground to surroundings	
Land Vegetation				

3. Methodology

3.1. Simulation Tool

With the increasing maturity of computer and CFD technologies, numerical simulation methods have been widely used in outdoor thermal environment research [14,15,17,33]. In this paper, we used the CFD software ENVI-met as a simulation tool. ENVI-met can accurately simulate the surface-plant-air interactions in an urban environment and has been fully recognized in the field of outdoor micro-environment simulation [2,28,34–38]. To validate the applicability of ENVI-met in Nanjing city, we conducted a field experiment (see in Appendix A), which revealed that the ENVI-met can be applied to this study.

3.2. Software Model

3.2.1. Atmospheric Model

1. Outdoor airflow

The control equations for outdoor airflow are the non-hydrostatic incompressible Navier-Stokes equations [39]:

$$\frac{\partial u}{\partial t} + u_i \frac{\partial u}{\partial x_i} = -\frac{\partial p'}{\partial x} + K_m \left(\frac{\partial^2 u}{\partial {x_i}^2} \right) + f(v - v_g) - S_u \tag{1}$$

$$\frac{\partial v}{\partial t} + u_i \frac{\partial v}{\partial x_i} = -\frac{\partial p}{\partial y} + K_m \left(\frac{\partial^2 v}{\partial {x_i}^2} \right) - f(u - u_g) - S_v \tag{2}$$

$$\frac{\partial w}{\partial t} + u_i \frac{\partial w}{\partial x_i} = -\frac{\partial p}{\partial z} + K_m \left(\frac{\partial^2 w}{\partial {x_i}^2} \right) + g \frac{\theta(z)}{\theta_{ref}(z)} - S_w \tag{3}$$

$$\frac{\partial u}{\partial x} + \frac{\partial v}{\partial y} + \frac{\partial w}{\partial z} = 0 \tag{4}$$

where f $(= 10^4 s^{-1})$ is the Coriolis parameter; p' is the local disturbance pressure and θ is the air temperature at height z; K_m is the change rate of the kinematic viscosity coefficient; and g is the acceleration of gravity. The reference temperature θ_{ref} represents the meteorological condition of the macroscopic climate, which is obtained by averaging all of the grids except the building. u, v, w are the wind speed components in three directions. u_{i} is the Einstein summation $(u_{\mathrm{i}} = u, v, w, i = 1, 2, 3)$. S_{u}, S_{v}, and S_{w} represent the drag effect of the plant on the wind, which are described in References [40,41].

2. Air temperature and humidity

The air temperature θ and humidity q of the atmosphere are obtained by solving the following advection–diffusion equation:

$$\frac{\partial \theta}{\partial t} + u_i \frac{\partial \theta}{\partial x_i} = K_h \left(\frac{\partial^2 \theta}{\partial {x_i}^2} \right) + Q_h \tag{5}$$

$$\frac{\partial q}{\partial t} + u_i \frac{\partial q}{\partial x_i} = K_q \left(\frac{\partial^2 q}{\partial {x_i}^2} \right) + Q_q \tag{6}$$

where Q_h and Q_q represent the heat and vapor exchange, respectively, between the plant surface and surrounding environment and can be obtained from the vegetation model described below. K_h and K_q are coefficients for turbulent sensible heat and vapor exchange, respectively.

3. Turbulence

The atmospheric turbulence adopts a 1.5-order closed-equation system (E-ε equation) based on the work of Mellor and Yamada [42]:

$$\frac{\partial E}{\partial t} + u_i \frac{\partial E}{\partial x_i} = K_E \left(\frac{\partial^2 E}{\partial {x_i}^2} \right) + \mathrm{Pr} - Th + Q_E - \varepsilon \tag{7}$$

$$\frac{\partial \varepsilon}{\partial t} + u_i \frac{\partial \varepsilon}{\partial x_i} = K_\varepsilon \left(\frac{\partial^2 \varepsilon}{\partial {x_i}^2} \right) + c_1 \frac{\varepsilon}{E} \mathrm{Pr} - c_3 \frac{\varepsilon}{E} Th - c_2 \frac{\varepsilon^2}{E} + Q_\varepsilon \tag{8}$$

$$\mathrm{Pr} = K_m \left(\frac{\partial u_i}{\partial x_j} + \frac{\partial u_j}{\partial x_i} \right) \frac{\partial u_i}{\partial x_j} \tag{9}$$

$$Th = \frac{g}{\theta_{ref}(z)} K_h \frac{\partial \theta}{\partial z} \tag{10}$$

where E is the turbulent kinetic energy; ε is the dissipation rate; and c_1, c_2, and c_3 are the empirical coefficients with values of c_1 = 1.44, c_2 = 1.92, and c_3 = 1.44 according to the literature [43]. Pr and Th

represent the turbulent energy and its dissipation caused by wind shearing and thermal stratification, respectively. Q_E and Q_ε describe the turbulent energy generation and dissipation caused by plant leaves, respectively. The control equations refer to references [41,44].

3.2.2. Radiation Flux

In the three-dimensional model, the distributions of solar radiation and long-wave are affected by the ground, plants, buildings, and other factors. ENVI-met uses a series of attenuation coefficients to describe the effects of these factors. The values of the attenuation coefficients range between 0 and 1. The influences of plants on solar radiation and long-wave radiation are shown below [45]:

$$\sigma_{sw,dir} = exp(F \cdot LAI^*(z)) \tag{11}$$

$$\sigma_{sw,dif} = exp\big(F \cdot LAI\big(z, z_p\big)\big) \tag{12}$$

$$\sigma_{lw}^{\uparrow} = exp(F \cdot LAI(0, z)) \tag{13}$$

$$\sigma_{lw}^{\downarrow} = exp\big(F \cdot LAI\big(z, z_p\big)\big) \tag{14}$$

where $\sigma_{sw,dir}$, $\sigma_{sw,dif}$, $\sigma_{lw}^{\uparrow}$ and $\sigma_{lw}^{\downarrow}$ are attenuation coefficients describing the effects of vegetation on direct and diffuse short-wave radiation and on downward and upward long-wave radiation, respectively. *LAI** is the three-dimensional leaf area index. LAI is the one-dimensional vertical leaf area index of plants from the ground ($z = 0$) or the height of z to the top of the plant at z_p:

$$LAI(z, z + \Delta z) = \int_{z'}^{z'+\Delta z} LAD\big(z'\big)dz' \tag{15}$$

For direct solar radiation, ENVI-met accounts for the effect of the solar incident angle. If the observation point in the simulated area is completely blocked by the surrounding buildings or plants, then $\sigma_{sw,dir}$ is set to zero.

3.2.3. Vegetation Model

ENVI-met divides the plants with a height of z_p and root depth of z_r into 10 equidistant layers. Users can define the leaf area density (LAD) and root area density (RAD). ENVI-met also provides a three-dimensional modeling tool that allows the user to define the LAD of each grid occupied by the plant canopy to describe different canopy shapes and to obtain the LAD distribution.

The interactions between plant leaves and the surrounding air are mainly described by the heat flux $\left(J_{f,h}\right)$, evaporation flux $\left(J_{f,evap}\right)$, and transpiration flux:

$$J_{f,h} = 1.1{\gamma_a}^{-1}\left(T_f - T_a\right) \tag{16}$$

$$J_{f,evap} = {\gamma_a}^{-1}\Delta q \delta_c f_w + {\gamma_a}^{-1}(1 - \delta_c)\Delta q \tag{17}$$

$$J_{f,trans} = \delta_c(\gamma_a + \gamma_s)^{-1}(1 - f_w)\Delta q \tag{18}$$

$$\Delta q = q^* T_a - q_a \tag{19}$$

where T_a and T_f are the temperatures of the air and leaves, respectively; Δq is the difference in humidity between the plant leaf surface and air; δ_c is an index defining the occurrence of plant evapotranspiration ($\delta_c = 1$, occurs, $\delta_c = 0$, does not occur); γ_a is the aerodynamic resistance of leaves on airflow; f_w is the proportion of leaves with liquid water; and γ_s is the stomatal resistance of the plant. For more details on the Formulas (16)–(19) refer to reference [39].

4. Case Study

4.1. Case Setup

This study takes a residential area with underground parking in Nanjing, China as a research object. Nanjing is one of China's famous "stove cities", which exhibit strong heat island effects, with summer outdoor air temperature of up to 40 °C [32]. The scale of the underground space development in Nanjing is extensive, reaching 2450 × 10^4 m^2 in 2013 and anticipated to reach 5200 × 10^4 m^2 by 2020 according to the urban plan for Nanjing [24]. Two types of building layouts, namely, determinant and enclosed layouts, were considered; these layouts are extremely common in Nanjing (Figure 1) [46]. A single building has dimensions of 30 m (L) × 15 m (W) × 18 m (H), and the site area is 80 m × 80 m (6400 m^2). In practice, tall trees are rarely planted in the underground space development area, and the green coverage of small shrubs and lawns are typically very similar. Therefore, we selected three types of greening configurations, namely, lawns, large shrubs, and small trees, with the same green coverage rate to investigate the effects of greening configuration on the outdoor thermal environment, as shown in Figure 1.

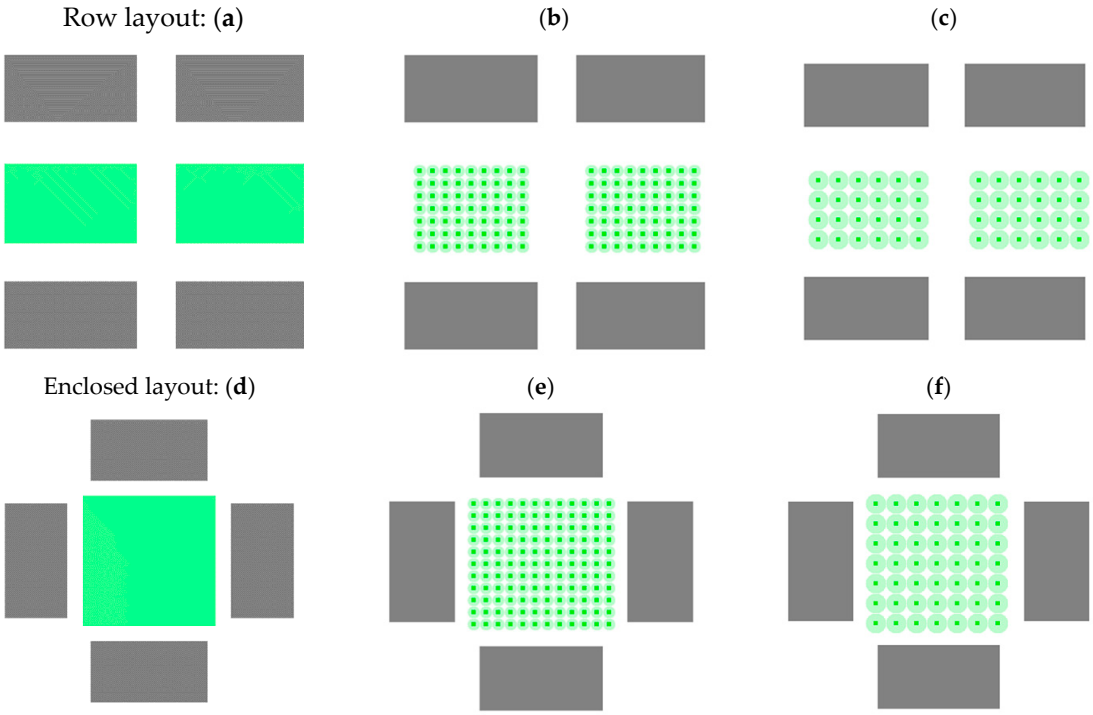

Figure 1. Case model. Row layout: (**a**) lawn; (**b**) large shrub; and (**c**) small tree; Enclosed layout: (**d**) lawn; (**e**) large shrub; and (**f**) small tree.

4.2. Numerical Method

The number of grids on each direction ($X \times Y \times Z$) is 80 × 80 × 30. The grid step in the horizontal direction ($X \times Y$) is 1 m × 1 m. The thermal environment quality at the height of pedestrians (1.5 m) is the main focus of this analysis. ENVI-met divides the lowest vertical grids into five equal-sized small grids (ΔZg = 0.2 Δz). Therefore, the grid step in the vertical direction was set to 7.5 m. Five nested grids were set to improve the stability of the numerical simulation. Typical summer weather data of Nanjing were chosen as the meteorological conditions for the simulation (Table 3). The parameters of the plants are provided in Table 4 [47].

Table 3. Meteorological parameters *.

Typical Weather Day	Relative Humidity (%)	Wind Speed (m/s)	Wind Direction (°)	Initial Atmospheric Temperature (K)	Outdoor Atmospheric Pressure (Pa)	Initial Time of Simulation	Total Simulation Time (h)
6.23 (Summer)	80	2.4	157.5	294.95	100,250	6:00	24

Note: * Wind direction of 0°, 90°, 180°, and 270° are for the north, east, south, and west, respectively.

Table 4. Parameters of the plants [47] *.

Model	Size (m) *	Leaf Area Index of Plant (LAD)									
		1	2	3	4	5	6	7	8	9	10
Lawn	0.2 H					0.3					
Large shrub	3 W × 3 L × 2 H				2.5				2.3	2.2	1.5
Small tree	5 W × 5 L × 10 H	0.15	0.15	0.15	0.15	0.65	2.15	2.18	2.05	1.72	0

Note: * L, W, and H are length, width, and height of the plants, respectively.

4.3. Evaluation Index

Air temperature, relative humidity, and wind speed are commonly used indexes for evaluating an outdoor thermal environment, as they can directly reflect the changes in such environments [17,24]. However, these indexes cannot accurately reflect the thermal comfort of humans. The evaluation of outdoor thermal comfort is more complex and difficult than that of indoor thermal comfort due to the complex radiation and wind environment outdoors [48]. At present, the most commonly used outdoor thermal comfort indexes include the outdoor standard effective temperature (OUT_SET *) [49,50], Predicted Mean Vote (PMV) [51], and PMV* [49], physiological equivalent temperature (PET) [52], and mean radiation temperature (MRT) [53].

In this study, we used the mean radiation temperature (MRT, T_{mrt}) to evaluate outdoor thermal comfort. The MRT refers to the surface temperature of an imaginary isothermal enclosed surface in which the radiant heat exchange capacity from the human body is equal to the actual amount of radiant heat exchange between the human body and the actual non-isothermal surface [54].

The MRT index was used because it has been widely used in evaluating outdoor thermal comfort on sunny days with a gentle breeze and can satisfy the requirement of this study [23,34,53] Theoretically, T_{mrt} applied to the outdoors is expressed as [51]:

$$T_{mrt} = \left[\frac{1}{\sigma}\left(\sum_{i=1}^{n} E_i F_i + + \frac{\partial_k}{\varepsilon_p}\sum_{i=1}^{n} D_i F_i + \frac{\partial_k}{\varepsilon_p} f_p I\right)\right]^{0.25} \quad (20)$$

where the environment is divided into n isothermal surfaces. For each isothermal surface, E_i (w/m^2) is the long-wave radiation; D_i (w/m^2) is the diffuse and short-wave radiation; F_i is the angle weighting factor; I (w/m^2) is the direct solar radiation normal to the surface; f_p is the surface emission coefficient, which is a function of the Sun's height, angle and position; ∂_k is the absorption coefficient of the irradiated surface of short-wave radiation (≈0.7); ε_p is the emissivity of the human body (≈0.97); and ε is the Stefan-Boltzmann constant ($\varepsilon = 5.67 \times 10^{-8}$ w/m^2·K^4).

In ENVI-met, by calculating the long wavelength of the total radiation intensity $E_t(z)$, the direct radiation $I_t(z)$ and the solar scattering radiation $D_t(z)$, the T_{mrt} of each grid point z can be obtained as [55]:

$$T_{mrt} = \left[\frac{1}{\sigma_B}\left(E_t(z) + \frac{\alpha k}{\varepsilon_p}(D_t(z) + I_t(z))\right)\right]^{0.25} \quad (21)$$

The surrounding environment consists of building surfaces, free atmosphere (sky), and ground. The software considers all radiation fluxes, such as direct solar radiation $I_t(z)$, the diffuse and diffusely

reflected solar radiation $D_t(z)$, and total long-wave radiation flux $E_t(z)$ from the atmosphere, ground, and walls.

In the calculation of $E_t(z)$, ENVI-met assumes that 50% of the total long-wave radiation comes from the sky and the surrounding buildings and the other 50% comes from the ground, which can be expressed as:

$$E_t(z) = 0.5[(1 - SVF(z))E_w + SVF(z)E_s]0.5E_g \quad (22)$$

The sky view factor SVF can be expressed as:

$$SVF = \frac{1}{360}\sum_{\alpha=0}^{360} cos\alpha(\pi) \quad (23)$$

The vertical angle α is determined by the obstruction at the azimuth angle π. To consider the exposure area of the relative shaded area, the heat flow from the ground E_g of point z can be calculated from the actual surface temperature T_g.

$$E_g = \varepsilon_g \sigma T_g^4 \quad (24)$$

The downward radiation flux E_s from the visible portion of the sky is calculated by SVF weighting. The long-wave radiation emitted by the wall E_w is calculated by averaging the surface temperature $\overline{T_w}$ of the building:

$$E_w(z) = (1 - SVF(z))\varepsilon_w \sigma \overline{T_w}^4 \quad (25)$$

The total diffuse radiation $D_t(z)$ is partially from the sky D_s and partially from the wall as the diffuse reflection of the solar radiation $(\alpha_m I(z))$ and is given by:

$$D_t(z) = (1 - SVF(z))\alpha_m I(z) + SVF(z)D_s \quad (26)$$

where α_m is the average albedo of the simulated area.

The heat radiation received by the human body $I_t(z)$ is a part of the direct solar radiation $I(z)$, which is calculated by

$$I_t(z) = f_p I(z) \quad (27)$$

where f_p is an empirical solar emission factor.

5. Results and Discussion

5.1. Airflow Field

Figure 2 shows the influence of the greening configuration on the outdoor wind velocity at the pedestrian level (1.5 m above ground, 12:00 a.m.). For each type of building layout, the outdoor wind fields for different greening configurations were very similar. In contrast, the building layout had a significant influence on the spatial distribution of the outdoor wind fields. The velocity of the southeast wind was decreased considerably due to the obstruction of buildings, and wind shadow areas formed at the leeward side of the buildings. In addition, adjacent buildings led to a funneling effect, which increased the local wind velocity.

The temporal profiles of the average wind velocity for different greening configurations were similar for the same building layout, whereas the wind fields for the enclosed layout were more stable than those for the row layout (Figure 3). These results can be explained in two ways. First, the buildings with enclosed layouts surrounded the underground space development area and blocked the wind from the southeast. Second, the buildings with row layouts shifted the wind to the underground space development area and increased air convection. These results indicate that the building layout can exert a greater influence on the temporal profile of average wind velocity than the greening configuration.

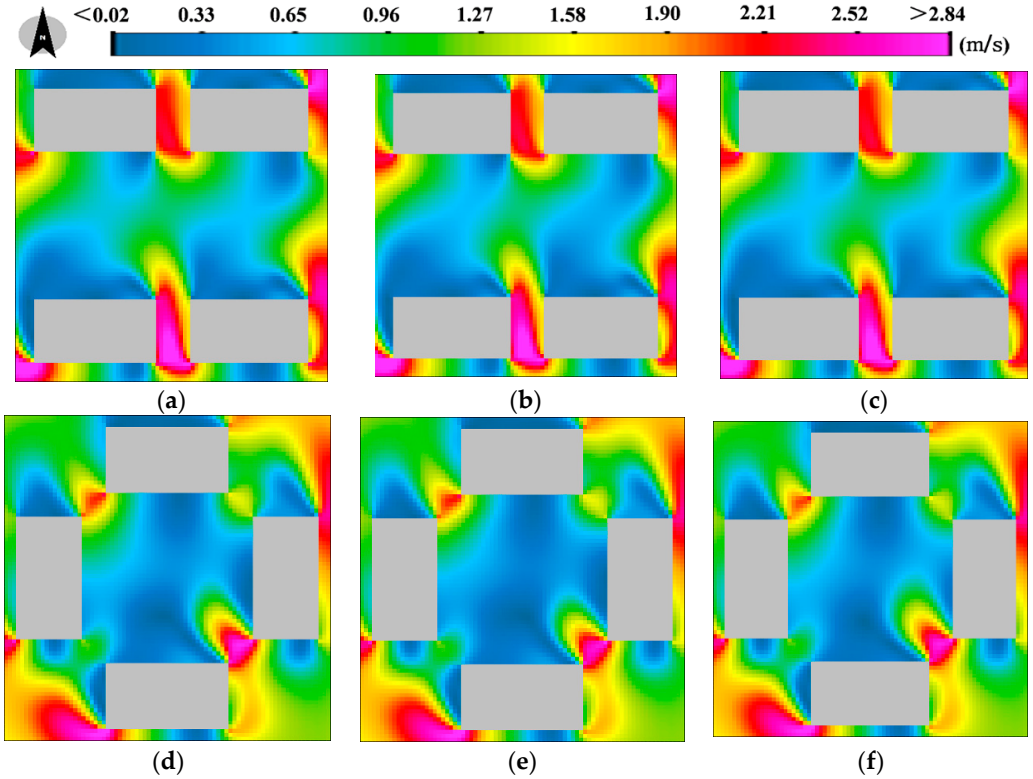

Figure 2. Influence of the greening configuration on the outdoor wind velocity at the pedestrian level (1.5 m above ground, 12:00 a.m.). Row layout: (**a**) lawn; (**b**) large shrub; and (**c**) small tree; Enclosed layout: (**d**) lawn; (**e**) large shrub; and (**f**) small tree.

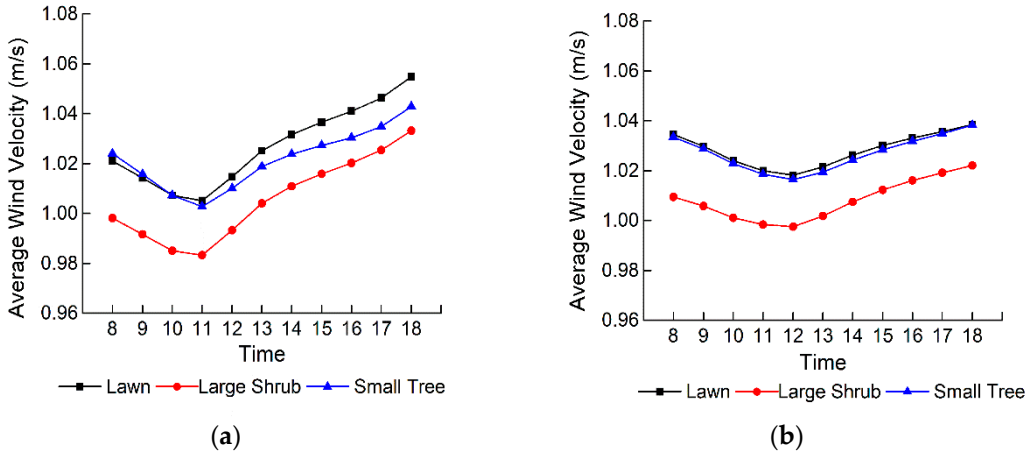

Figure 3. Change in the average wind velocity over time for different greening configurations and building layouts: (**a**) row layout; (**b**) enclosed layout (1.5 m above ground).

For each type of building layout, the average wind velocities for lawns were typically the highest, whereas the average wind velocities for large shrubs, not small trees, were lowest. There are two possible reasons for this result. First, with the same greening coverage, small trees were sparser than large shrubs, which led to a higher airflow. Second, the large shrubs at a height of 2 m above ground affected the airflow at the pedestrian level more than the small trees. The results indicate that for a given greening coverage, small trees are more favorable for air convection at the pedestrian level than large shrubs.

5.2. Air Temperature

Figure 4 shows the influence of the greening configuration on the outdoor air temperature at the pedestrian level (1.5 m above ground, 12:00 a.m.). For each type of building layout, the outdoor air temperature for large shrubs was typically the lowest, and the outdoor air temperature for lawns was similar to that for small trees. The results shown in Figure 3 reflect the differences in the mechanisms by which the greening configuration can affect the outdoor air temperature distribution. Dense shrubs can provide more shade than sparse trees and grasses, which can reduce the solar radiation received by the ground and further reduce the air temperature at the pedestrian level. Although grasses cannot provide the same amount of shade as large trees, they can reduce the ground surface temperature through photosynthesis and transpiration; thus, the reduction in the air temperature at the pedestrian level for lawns was similar to that for large trees.

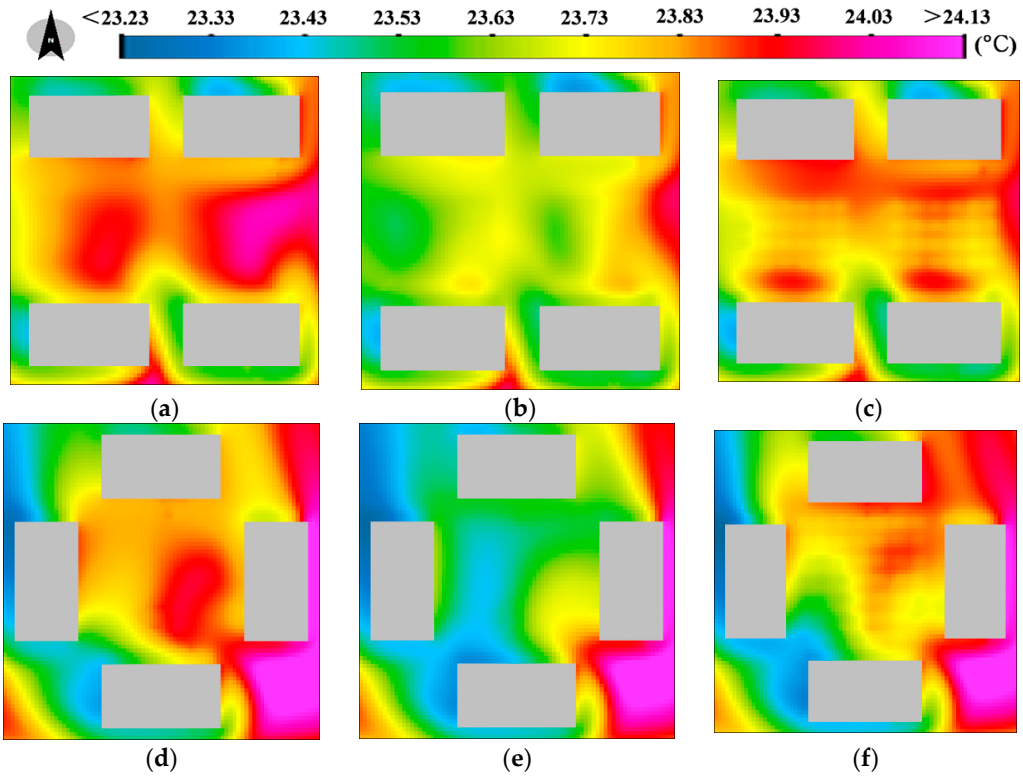

Figure 4. Influence of the greening configuration on the outdoor air temperature at the pedestrian level (1.5 m above ground, 12:00 a.m.). Row layout: (**a**) lawn; (**b**) large shrub; and (**c**) small tree; Enclosed layout: (**d**) lawn; (**e**) large shrub; and (**f**) small tree.

The average air temperatures at the pedestrian level for different greening configurations and building layouts changed according to a similar temporal profile, which increased over time and reached its maximum at 16:00 p.m. (Figure 5). For each type of building layout, the average air temperature for large shrubs was the lowest. Taking the row layout as an example, the maximum average air temperature for large shrubs was 0.20 °C (15:00 p.m.) and 0.14 °C (14:00 p.m.) lower than those for lawns and small trees, respectively. These results indicate that in the underground space development area, the heat island effects can be effectively reduced by implementing an OTUS that satisfies the requirement of planting large shrubs.

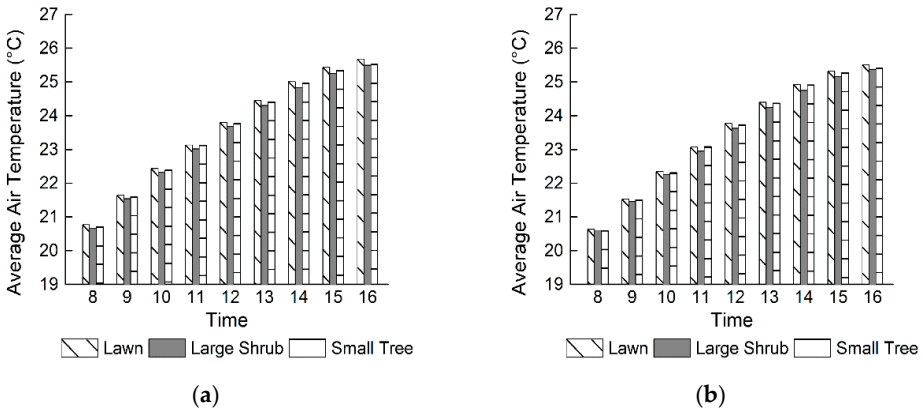

Figure 5. Comparison of the average air temperature by hour for different green configurations and building layouts: (**a**) row layout; (**b**) enclosed layout (1.5 m above ground).

5.3. Relative Humidity

Figure 6 shows the influence of the greening configuration on the outdoor relative humidity at the pedestrian level (1.5 m above ground, 12:00 a.m.). For each type of building layout, the pedestrian-level relative humidity values for lawns were consistently the lowest. The relative humidity values for small trees were slightly higher than those for large shrubs.

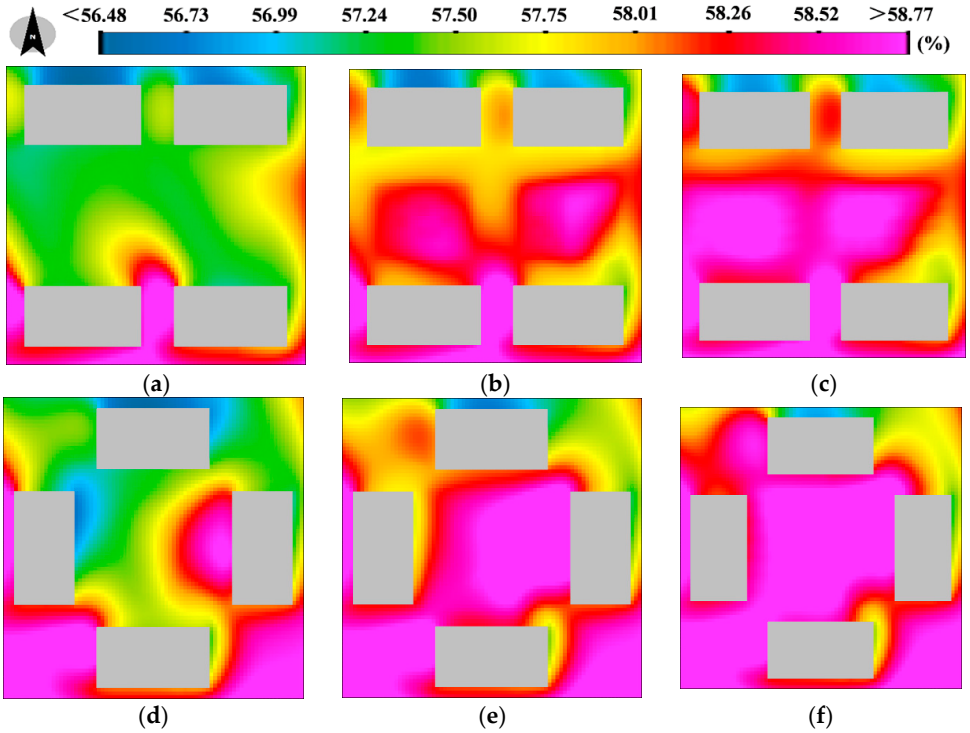

Figure 6. Influence of the greening configuration on the outdoor relative humidity at the pedestrian level (1.5 m above ground, 12:00 a.m.). Row layout: (**a**) lawn; (**b**) large shrub; and (**c**) small tree; Enclosed layout: (**d**) lawn; (**e**) large shrub; and (**f**) small tree.

The average relative humidity for different greening configurations and building layouts changed with a similar temporal profile, decreasing over time and reaching its minimum at 16:00 p.m. (Figure 7). For each type of building layout, the average relative humidity for small trees was the highest, followed by those for large shrubs and lawns. The differences between the average relative humidity of the

three types of greening configurations were extremely small (0.06%–0.67%). These results indicate that changes in the greening configuration have only a slight influence on the outdoor pedestrian-level relative humidity for a given greening coverage.

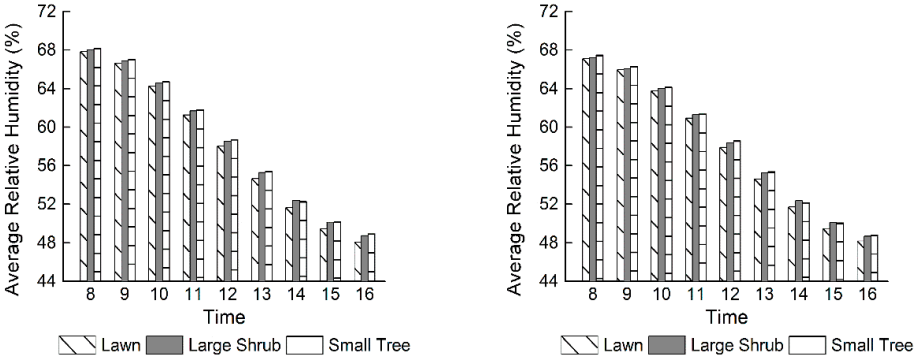

Figure 7. Comparison of the average relative humidity by hour for different green configurations and building layouts: (**a**) row layout; (**b**) enclosed layout (1.5 m above ground).

5.4. Mean radiation temperature (MRT)

Figure 8 shows the influence of the greening configuration on the outdoor MRT at the pedestrian level (1.5 m above ground, 12:00 a.m.). For each type of building layout, the MRT distributions in the underground space development area were significantly lower than those in other areas due to the cooling effect of greening. The results indicate that each of the three greening types can reduce the outdoor pedestrian-level MRT significantly.

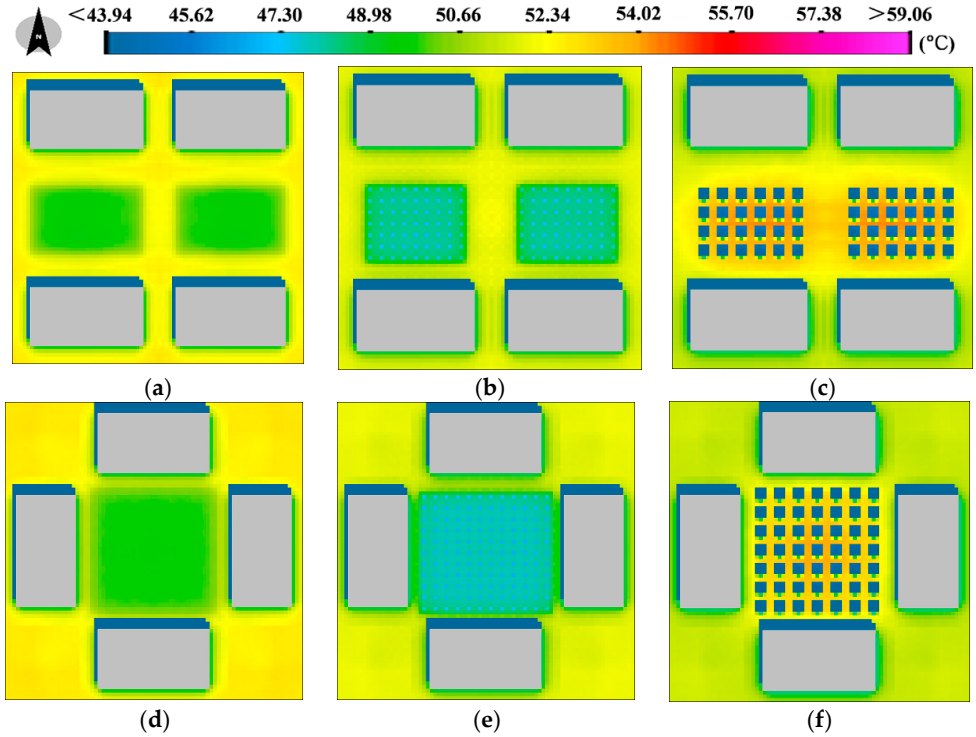

Figure 8. Influence of the greening configuration on the mean radiation temperature (MRT) at the pedestrian level (1.5 m above ground, 12:00 a.m.). Row layout: (**a**) lawn; (**b**) large shrub; and (**c**) small tree; Enclosed layout: (**d**) lawn; (**e**) large shrub; and (**f**) small tree.

Further observations indicated that with the same greening coverage, the distribution of outdoor pedestrian-level MRT for lawns was similar to that for large shrubs, and both were different from that for small trees. The MRT values for lawns were typically higher than those for large shrubs due to the lack of shade. The MRT distributions for lawns and large shrubs were more uniform than that for small trees in the underground space development area because the grasses and large shrubs were densely planted, whereas the small trees were sparsely planted.

For each type of building layout, the temporal profiles of the average outdoor MRT at the pedestrian level for different greening configurations were similar (Figure 9a,b). The influence of the greening configuration on the pedestrian-level thermal comfort was closely related to the change in the solar elevation angle. Before noon, the differences between the average MRT values for different greening configurations decreased with increases in the solar elevation angle. These values were most similar at noon. After noon, the differences between these values increased with the decreases in the solar elevation angle. These results indicate that the geographical location of the residential district and the movement of local sun should be considered in the design of OTUSs and ground greening configurations to effectively improve outdoor pedestrian-level thermal comfort.

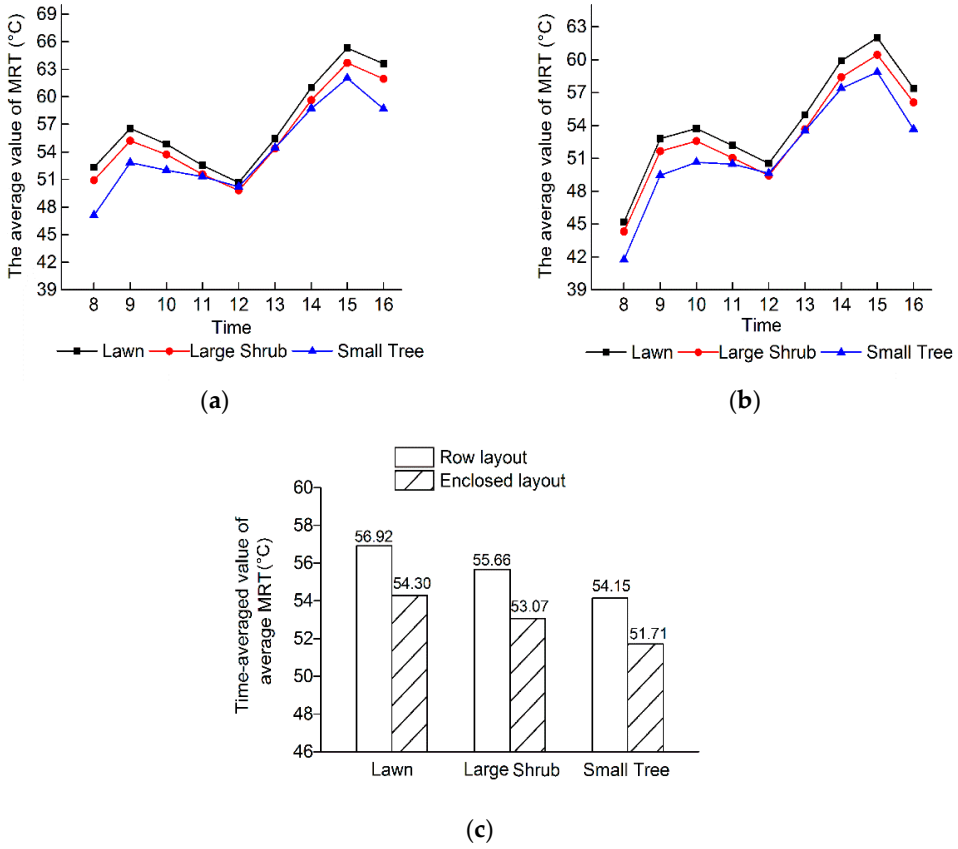

Figure 9. Simulation results of the MRT: (**a**) hourly values of the MRT for the row layout; (**b**) hourly values of the MRT for the enclosed layout; (**c**) time-averaged value of the average MRT for the two types of building layouts (8:00–16:00, Δt = 1 h, 9 time points).

The time-averaged values of the average MRT for different greening configurations for the two types of building layouts were obtained by averaging the average MRT values from 8:00 a.m. to 16:00 p.m. (nine time points) (see Figure 9c). For each type of building layout, the time-averaged value for lawns was highest, followed by those for large shrubs and small trees. The time-averaged value for small trees in the row layout was 2.77 °C and 1.51 °C lower than those for lawns and large shrubs, respectively, and the corresponding differences in the enclosed layout were 2.59 °C and 1.36 °C.

The above results indicate that for a given greening coverage in Nanjing, small trees are the most favorable greening configuration for improving outdoor thermal comfort at the pedestrian level, followed by large shrubs and lawns. Thus, the OTUS should be designed such that the requirement of planting small trees is met. If this requirement cannot be satisfied, tree wells can be set up or soil can be added on top of underground structures to plant small trees and thus provide an OTUS that can satisfy the requirement of planting large shrubs in other areas.

6. Conclusions

In this study, we chose two residential areas with row and enclosed layouts in Nanjing, China, as the research objects and used the CFD software ENVI-met to quantitatively analyze the outdoor pedestrian-level thermal environment changes under three greening configurations—lawns, large shrubs, and small trees—with the same green coverage and to provide suggestions regarding the design of the OTUS based on the simulation results. The results of this study led to the following conclusions:

(1) The building layout can exert a greater influence on the temporal profile of the average wind velocity than the greening configuration. For a given greening coverage, the average wind velocities for lawns were typically the highest, and small trees were more favorable for air convection at the pedestrian level than large shrubs.

(2) The heat island effects in an underground space development area can be effectively reduced if the OTUS satisfies the requirement for planting large shrubs. For a given greening coverage, changes in the greening configuration have only a slight influence on the outdoor relative humidity at the pedestrian level.

(3) Lawns, large shrubs, and small trees can all reduce the outdoor MRT at the pedestrian level significantly. For a given greening coverage in Nanjing, small trees are the most favorable greening configuration for improving outdoor thermal comfort at the pedestrian level, followed by large shrubs and lawns.

(4) The OTUS should be designed to satisfy the requirement of planting small trees. If this requirement cannot be adequately met, individuals can also set up tree wells or add soil on top of underground structures to plant small trees, and establish an OTUS that can satisfy the requirement of planting large shrubs in other areas.

Acknowledgments: This study was supported by the National Natural Science Foundation of China (Grant No. 51478463).

Author Contributions: XiaoChao Su, Hao Cai, and Zhilong Chen conceived and designed the study. Xiaochao Su and Qilin Feng performed the numerical simulations and result analyses. Xiaochao Su and Hao Cai wrote the paper. Zhilong Chen and Qilin Feng reviewed and edited the manuscript. All authors read and approved the manuscript.

Conflicts of Interest: The authors declare no conflict of interest.

Appendix A. Validation of ENVI-Met

The field experiments were conducted between 8:00 a.m. and 5:00 p.m. on 17 October 2015. We measured different underlying surface temperatures in a residential area of Nanjing, China, using laser range finder (measurement accuracy 0.1 °C) and thermal infrared imager (measurement accuracy 0.1 m). The weather data of that day were used as the inputs of ENVI-met (Table A1).

Table A1. Weather data of Nanjing city on 17 October 2015.

Initial Atmospheric Temperature (K)	Relative Humidity (%)	Wind Velocity (m/s)	Wind Direction (°)	Grid Numbers ($X \times Y \times Z$)	Initial Time of Simulation	Simulation Time (h)
288.45	86.2	2.3	135	$80 \times 100 \times 30$	5:00 a.m.	24

Six monitor points were arranged on different underlying surfaces (Figure A1), including tree (Point 1), permeable pavement (Point 2), pond (Point 3), sintered granite (Point 4), lawn (Point 5), and asphalt road (Point 6). Figure A2 shows the real scenes and thermal image maps at 9:00 a.m. of the six monitor points.

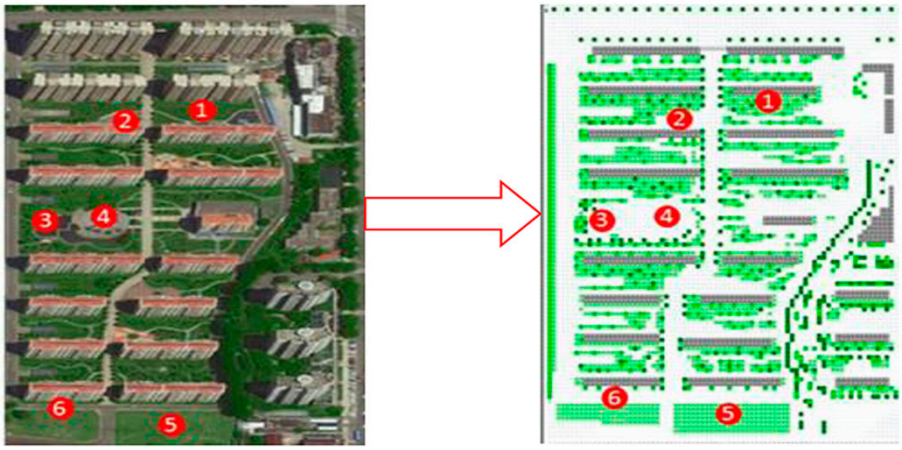

Figure A1. Layouts of monitor points and simulation model.

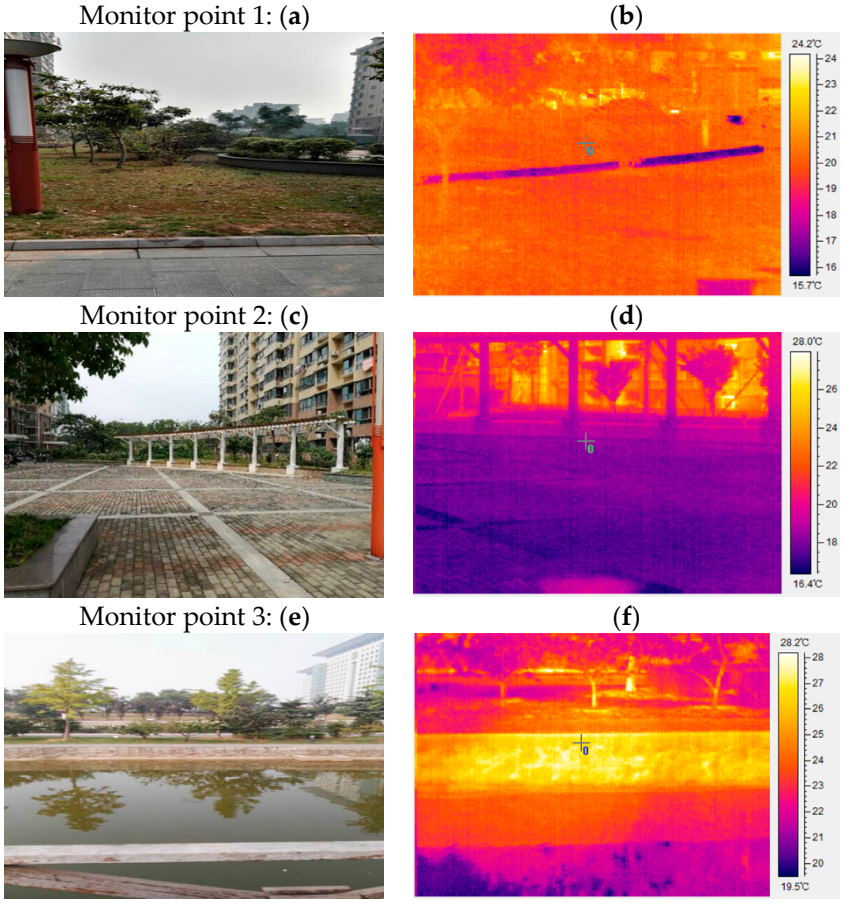

Figure A2. *Cont.*

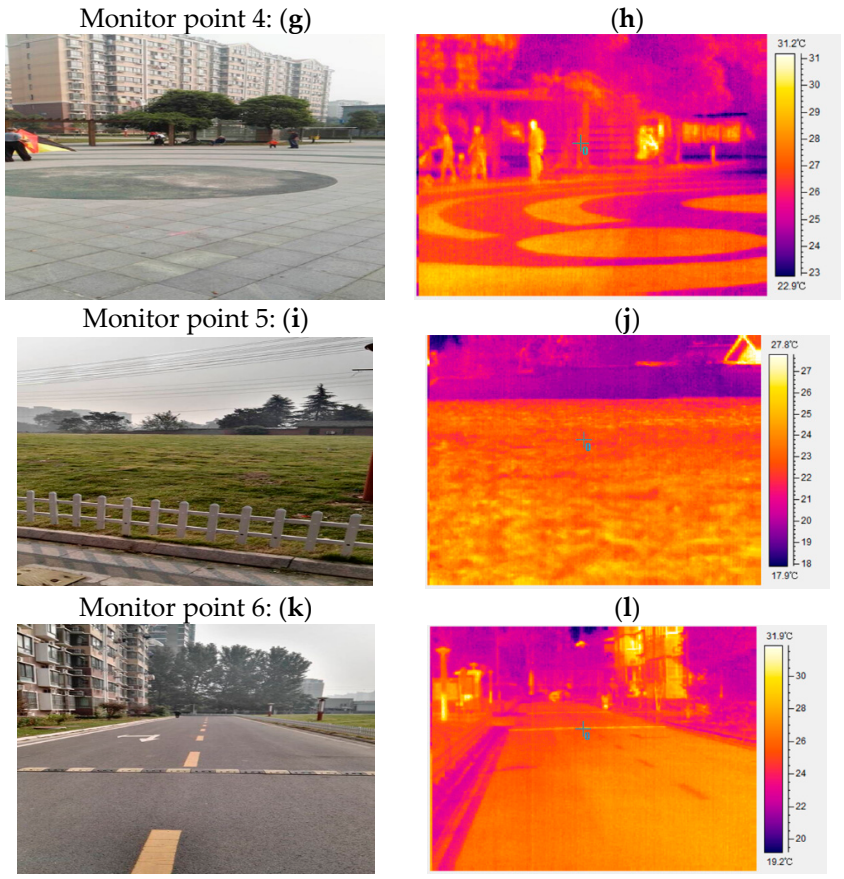

Figure A2. Real scenes and thermal image maps at 9:00 a.m. of the six monitor points. (**a**,**c**,**e**,**g**,**i**,**k**) are the real scenes of six monitor points, respectively; (**b**,**d**,**f**,**h**,**j**,**l**) are thethermal image maps at 9:00 a.m. of six monitor points, respectively.

The comparison of measured and simulated underlying surface temperature (Figure A3) shows that the relative errors of measurements were less than 10% at most time points. Only at Point 1 and Point 2, were the relative errors larger than 10%, which may have been caused by the errors existing in weather data. The field experiments validated that the accuracy of ENVI-met can meet the requirements of this study.

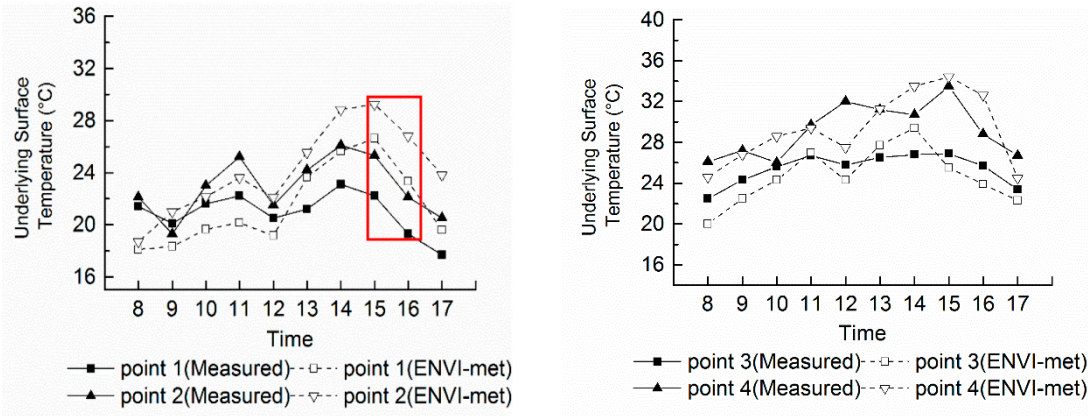

(**a**) (**b**)

Figure A3. *Cont.*

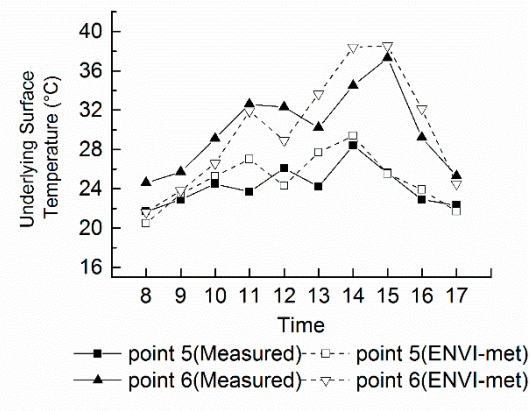

(**c**)

Figure A3. Comparison of measured and simulated underlying surface temperatures of six monitor points. (**a**) Points 1 and 2; (**b**) points 3 and 4; (**c**) points 5 and 6.

References

1. Hong, B.; Lin, B.R. Numerical studies of the outdoor wind environment and thermal comfort at pedestrian level in housing blocks with different building layout patterns and trees arrangement. *Renew. Energy* **2015**, *73*, 18–27. [CrossRef]
2. Yang, F.; Lau, S.S.Y.; Qian, F. Thermal comfort effects of urban design strategies in high-rise urban environments in a sub-tropical climate. *Archit. Sci. Rev.* **2011**, *54*, 285–304. [CrossRef]
3. Lin, T.P.; Matzarakis, A.; Hwang, R.L. Shading effect on long-term outdoor thermal comfort. *Build. Environ.* **2010**, *45*, 213–221. [CrossRef]
4. Lai, D.Y.; Guo, D.H.; Hou, Y.F.; Lin, C.Y.; Chen, Q.Y. Studies of outdoor thermal comfort in northern China. *Build. Environ.* **2014**, *77*, 110–118. [CrossRef]
5. Yang, X.S.; Zhao, L.H.; Bruse, M.; Meng, Q.L. An integrated simulation method for building energy performance assessment in urban environments. *Energy Build.* **2012**, *54*, 243–251. [CrossRef]
6. Wong, K.V.; Paddon, A.; Jimenez, A. Review of world urban heat islands: Many linked to increased mortality. *J. Energy Resour. Technol.-Trans. ASME* **2013**, *135*, 11. [CrossRef]
7. Robine, J.M.; Cheung, S.L.K.; Le Roy, S.; Van Oyen, H.; Griffiths, C.; Michel, J.P.; Herrmann, F.R. Death toll exceeded 70,000 in europe during the summer of 2003. *C. R. Biol.* **2008**, *331*, 171–175. [CrossRef] [PubMed]
8. Conti, S.; Meli, P.; Minelli, G.; Solimini, R.; Toccaceli, V.; Vichi, M.; Beltrano, C.; Perini, L. Epidemiologic study of mortality during the summer 2003 heat wave in italy. *Environ. Res.* **2005**, *98*, 390–399. [CrossRef] [PubMed]
9. Changnon, S.A.; Kunkel, K.E.; Reinke, B.C. Impacts and responses to the 1995 heat wave: A call to action. *Bull. Am. Meteorol. Soc.* **1996**, *77*, 1497–1506. [CrossRef]
10. Hong, B.; Lin, B.R.; Wang, B.; Li, S.H. Optimal design of vegetation in residential district with numerical simulation and field experiment. *J. Cent. South Univ. Technol.* **2012**, *19*, 688–695. [CrossRef]
11. Dimoudi, A.; Nikolopoulou, M. Vegetation in the urban environment: Microclimatic analysis and benefits. *Energy Build.* **2003**, *35*, 69–76. [CrossRef]
12. Chen, A.L.; Yao, X.A.; Sun, R.H.; Chen, L.D. Effect of urban green patterns on surface urban cool islands and its seasonal variations. *Urban For. Urban Green.* **2014**, *13*, 646–654. [CrossRef]
13. Sugawara, H.; Shimizu, S.; Takahashi, H.; Hagiwara, S.; Narita, K.; Mikami, T.; Hirano, T. Thermal influence of a large green space on a hot urban environment. *J. Environ. Qual.* **2016**, *45*, 125–133. [CrossRef] [PubMed]
14. Ooka, R.; Chen, H.; Kato, S. Study on optimum arrangement of trees for design of pleasant outdoor environment using multi-objective genetic algorithm and coupled simulation of convection, radiation and conduction. *J. Wind Eng. Ind. Aerodyn.* **2008**, *96*, 1733–1748. [CrossRef]
15. Hong, B.; Lin, B.R.; Hu, L.H.; Li, S.H. Optimal tree design for sunshine and ventilation in residential district using geometrical models and numerical simulation. *Build. Simul.* **2011**, *4*, 351–363. [CrossRef]

16. Lee, H.; Mayer, H.; Chen, L. Contribution of trees and grasslands to the mitigation of human heat stress in a residential district of freiburg, southwest germany. *Landsc. Urban Plan.* **2016**, *148*, 37–50. [CrossRef]
17. Lin, B.R.; Li, X.F.; Zhu, Y.X.; Qin, Y.G. Numerical simulation studies of the different vegetation patterns' effects on outdoor pedestrian thermal comfort. *J. Wind Eng. Ind. Aerodyn.* **2008**, *96*, 1707–1718. [CrossRef]
18. Ng, E.; Chen, L.; Wang, Y.N.; Yuan, C. A study on the cooling effects of greening in a high-density city: An experience from hong kong. *Build. Environ.* **2012**, *47*, 256–271. [CrossRef]
19. Chen, Z. *Overall Planning of Urban Underground Space*; Southeast University Press: Nanjing, China, 2011. (In Chinese)
20. Dai, P.; Wei, X.T. The study of the method of China cities underground space development and utilization. *Appl. Mech. Mater.* **2012**. [CrossRef]
21. Broere, W. Urban underground space: Solving the problems of today's cities. *Tunn. Undergr. Space Technol.* **2016**, *55*, 245–248. [CrossRef]
22. Hunt, D.V.L.; Makana, L.O.; Jefferson, I.; Rogers, C.D.F. Liveable cities and urban underground space. *Tunn. Undergr. Space Technol.* **2016**, *55*, 8–20. [CrossRef]
23. Yang, X.B.; Chen, Z.L.; Cai, H. The research on the impact of the underground parking to the microclimate in residential quarter. In *Sustainable Development of Industry and Economy, Pts 1 and 2*; Xu, Q., Li, H., Li, Q., Eds.; Trans Tech Publications Ltd.: Stafa-Zurich, Switzerland, 2014; Volume 869–870, pp. 178–184.
24. Yang, X.B.; Chen, Z.L.; Cai, H.; Ma, L.J. A framework for assessment of the influence of China's urban underground space developments on the urban microclimate. *Sustainability* **2014**, *6*, 8536–8566. [CrossRef]
25. China National Building Waterproof Association. *JGJ 155-2013 Technical Specification for Planted Roof*; China Architecture & Building Press: Beijing, China, 2013. (In Chinese)
26. Beijing Municipal Bureau of Parks. *Code for Design of Parks*; China Architecture & Building Press: Beijing, China, 1993. (In Chinese)
27. Chen, L.; Ng, E. Simulation of the effect of downtown greenery on thermal comfort in subtropical climate using pet index: A case study in hong kong. *Archit. Sci. Rev.* **2013**, *56*, 297–305. [CrossRef]
28. Shahidan, M.F.; Jones, P.J.; Gwilliam, J.; Salleh, E. An evaluation of outdoor and building environment cooling achieved through combination modification of trees with ground materials. *Build. Environ.* **2012**, *58*, 245–257. [CrossRef]
29. Srivanit, M.; Hokao, K. Evaluating the cooling effects of greening for improving the outdoor thermal environment at an institutional campus in the summer. *Build. Environ.* **2013**, *66*, 158–172. [CrossRef]
30. Wong, N.H.; Jusuf, S.K.; La Win, A.A.; Thu, H.K.; Negara, T.S.; Wu, X.C. Environmental study of the impact of greenery in an institutional campus in the tropics. *Build. Environ.* **2007**, *42*, 2949–2970. [CrossRef]
31. Yang, X.S.; Zhao, L.H.; Bruse, M.; Meng, Q.L. Evaluation of a microclimate model for predicting the thermal behavior of different ground surfaces. *Build. Environ.* **2013**, *60*, 93–104. [CrossRef]
32. Huang, L.M.; Li, H.T.; Zha, D.H.; Zhu, J.Y. A fieldwork study on the diurnal changes of urban microclimate in four types of ground cover and urban heat island of Nanjing, China. *Build. Environ.* **2008**, *43*, 7–17. [CrossRef]
33. Robitu, M.; Musy, M.; Inard, C.; Groleau, D. Modeling the influence of vegetation and water pond on urban microclimate. *Sol. Energy* **2006**, *80*, 435–447. [CrossRef]
34. Ali-Toudert, F.; Mayer, H. Numerical study on the effects of aspect ratio and orientation of an urban street canyon on outdoor thermal comfort in hot and dry climate. *Build. Environ.* **2006**, *41*, 94–108. [CrossRef]
35. Ali-Toudert, F.; Mayer, H. Effects of asymmetry, galleries, overhanging facades and vegetation on thermal comfort in urban street canyons. *Sol. Energy* **2007**, *81*, 742–754. [CrossRef]
36. Middel, A.; Hab, K.; Brazel, A.J.; Martin, C.A.; Guhathakurta, S. Impact of urban form and design on mid-afternoon microclimate in phoenix local climate zones. *Landsc. Urban Plan.* **2014**, *122*, 16–28. [CrossRef]
37. Kong, F.; Sun, C.F.; Liu, F.F.; Yin, H.W.; Jiang, F.; Pu, Y.X.; Cavan, G.; Skelhorn, C.; Middel, A.; Dronova, I. Energy saving potential of fragmented green spaces due to their temperature regulating ecosystem services in the summer. *Appl. Energy* **2016**, *183*, 1428–1440. [CrossRef]
38. Yang, X.S.; Zhao, L.H. Diurnal thermal behavior of pavements, vegetation, and water pond in a hot-humid city. *Buildings* **2016**, *6*, 12. [CrossRef]
39. Bruse, M.; Fleer, H. Simulating surface-plant-air interactions inside urban environments with a three dimensional numerical model. *Environ. Model. Softw.* **1998**, *13*, 373–384. [CrossRef]

40. Yamada, T. A numerical model study of turbulence airflow in and above a forest canopy. *J. Meteorol. Soc. Jpn.* **1982**, *60*, 439–454. [CrossRef]
41. Liu, J.; Chen, J.M.; Black, T.A.; Novak, M.D. *E*-ε modelling of turbulent air flow downwind of a model forest edge. *Bound. Layer Meteorol.* **1996**, *77*, 21–44. [CrossRef]
42. Mellor, G.L.; Yamada, T. A simulation of the wangara atmospheric boundary layer data. *J. Atmos. Sci.* **1975**, *32*, 2309–2329.
43. Launder, B.E.; Spalding, D.B. The numerical computation of turbulent flows. *Comput. Methods Appl. Mech. Eng.* **1974**, *3*, 269–289. [CrossRef]
44. Wilson, J.D. A second-order closure model for flow through vegetation. *Bound. Layer Meteorol.* **1988**, *42*, 371–392. [CrossRef]
45. Bruse, M. Development of a Microscale Model for the Calculation of Surface Temperatures in Structured Terrain. Ph.D. Thesis, University of Bochum, Bochum, Germany, 1995.
46. Li, M. The Study of the Influence of Space Morphology on Wind Environment in Residential Building in Nanjing Residential Area. Master's Thesis, Southeast University, Nanjing, China, May 2016.
47. Plant Database PLANTS.DAT. Available online: http://www.envi-met.info/documents/onlinehelpv3/helpindex.htm (accessed on 25 April 2017).
48. Höppe, P. Different aspects of assessing indoor and outdoor thermal comfort. *Energy Build.* **2002**, *34*, 661–665. [CrossRef]
49. Gagge, A.P. A standard predictive index of human response to the thermal environment. *Ashrae Trans.* **1986**, *92*, 709–731.
50. Dear, R.D.; Pickup, J. An outdoor thermal comfort index (out-set*)—Part I—The model and its assumptions. In Proceedings of the International Congress of Biometeorology and International Conference on Urban Climatology, Sydney, Australia, 8–12 November 1999.
51. Fanger, P.O. Thermal comfort. Analysis and applications in environmental engineering. In *Thermal Comfort: Analysis & Applications in Environmental Engineeri*; Danish Technical Press: Copenhagen, Denmark, 1970.
52. Mayer, H.; Hoppe, P. Thermal comfort of man in different urban environments. *Theor. Appl. Climatol.* **1987**, *38*, 43–49. [CrossRef]
53. Hoppe, P. The physiological equivalent temperature—A universal index for the biometeorological assessment of the thermal environment. *Int. J. Biometeorol.* **1999**, *43*, 71–75. [CrossRef] [PubMed]
54. International Organization for Standardization. *ISO 7726:1998—Ergonomics of the Thermal Environment—Instrument for Measuring Physical Quantities*; International Organization for Standardization: Geneva, Switzerland, 1998.
55. Bruse, M. *The Influences of Local Environmental Design on Microclimate-Development of a Prognostic Numerical Model Envi-Met for the Simulation of Wind, Temperature and Humidity Distribution in Urban Structures*; Temperature and Humidity Distribution in Urban Structures; Institute of Geography, University of Bochum: Bochum, Germany, 1999. (In German)